JACS
JOURNAL OF THE AMERICAN CHEMICAL SOCIETY
Article
Cite This: J. Am. Chem. Soc. XXXX, XXX, XXX−XXX
pubs.acs.org/JACS

Radical Rebound Hydroxylation Versus H-Atom Transfer in Non-Heme Iron(III)-Hydroxo Complexes: Reactivity and Structural Differentiation

Michael J. Drummond,[†] Courtney L. Ford,[†] Danielle L. Gray,[†] Codrina V. Popescu,[‡] and Alison R. Fout*[,†]

[†]School of Chemical Sciences, University of Illinois at Urbana—Champaign, 600 South Mathews Avenue, Urbana, Illinois 61801, United States

[‡]Department of Chemistry, University of Saint Thomas, 2115 Summit Avenue, Saint Paul, Minnesota 55105, United States

Supporting Information

ABSTRACT: The characterization of high-valent iron centers in enzymes has been aided by synthetic model systems that mimic their reactivity or structural and spectral features. For example, the cleavage of dioxygen often produces an iron(IV)-oxo that has been characterized in a number of enzymatic and synthetic systems. In non-heme 2-oxogluterate dependent (iron-2OG) enzymes, the ferryl species abstracts an H-atom from bound substrate to produce the proposed iron(III)-hydroxo and caged substrate radical. Most iron-2OG enzymes perform a radical rebound hydroxylation at the site of the H-atom abstraction (HAA); however, recent reports have shown that certain substrates can be desaturated through the loss of a second H atom at a site adjacent to a heteroatom (N or O) for most native desaturase substrates. One proposed mechanism for the removal of the second H-atom involves a polar-cleavage mechanism (electron transfer-proton transfer) by the iron(III)-hydroxo, as opposed to a second HAA. Herein we report the synthesis and characterization of a series of iron complexes with hydrogen bonding interactions between bound aquo or hydroxo ligands and the secondary coordination sphere in ferrous and ferric complexes. Interconversion among the iron species is accomplished by stepwise proton or electron addition or subtraction, as well as H-atom transfer (HAT). The calculated bond dissociation free energies (BDFEs) of two ferric hydroxo complexes, differentiated by their noncovalent interactions and reactivity, suggest that neither complex is capable of activating even weak C−H bonds, lending further support to the proposed mechanism for desaturation in iron-2OG desaturase enzymes. Additionally, the ferric hydroxo species are differentiated by their reactivity toward performing a radical rebound hydroxylation of triphenylmethylradical. Our findings should encourage further study of the desaturase systems that may contain unique H-bonding motifs proximal to the active site that help bias substrate desaturation over hydroxylation.

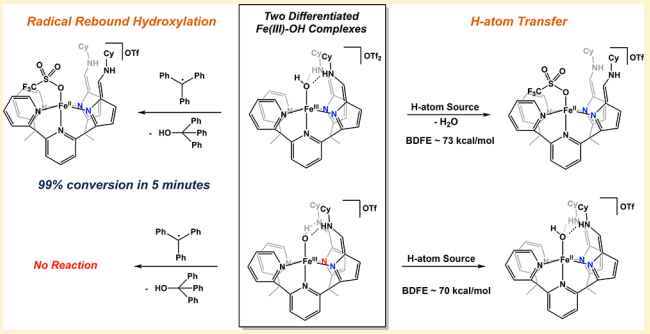

INTRODUCTION

The characterization of short-lived intermediates in enzymatic cycles has often been aided by synthetic model systems with well-defined molecular scaffolds. For example, extensive work has detailed the spectroscopic properties, structural parameters, and reactivity trends of iron(IV)-oxo species in synthetic systems.[1−5] These findings have been invaluable in assigning key ferryl intermediates in nonheme 2-oxogluterate dependent (iron-2OG) enzymes that activate dioxygen.[6−8]

The ferryl functionality, resulting from the cleavage of dioxygen, has been identified in enzymatic systems using stopped-flow UV−visible and Mössbauer spectroscopies.[9−11] The proposed subsequent step involves hydrogen atom abstraction (HAA) from a bound organic substrate to form a caged substrate radical and an iron(III)-hydroxo species (Figure 1, center). This ferrichydroxo species, which has not been observed spectroscopically in enzymatic systems,[10,12] can then perform a radical rebound reaction to hydroxylate the substrate (Figure 1, right). Computational studies have estimated an activation barrier of 1−4 kcal/mol for substrate hydroxylation, with an intermediate lifetime of ∼20 ps,[13−17] but attempts to trap an intermediate using a radical clock have been unsuccessful.

It has recently been shown that the presence of an arginine residue in proximity of the enzyme active site is necessary to properly position the oxo moiety and substrate for hydroxylation.[18] Alternatively, the absence of the arginine in proximity of the active site, among other factors such as the presence of adjacent heteroatoms (N or O) in substrate, may favor alternate reactivity, such as substrate desaturation (Figure 1, left),[19−21] ring formation,[22] decarboxylation,[23] or halogen-

Received: February 8, 2019

DOI: 10.1021/jacs.9b01516
J. Am. Chem. Soc. XXXX, XXX, XXX−XXX

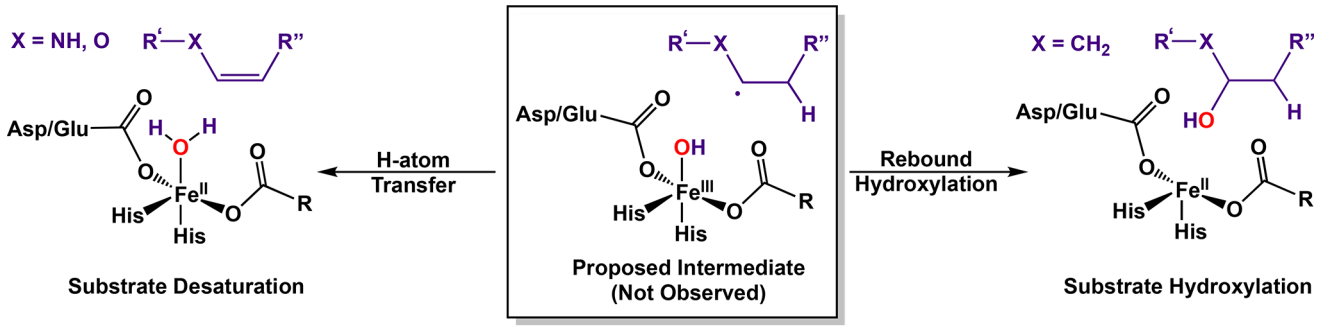

Figure 1. Alternative reactivity pathways from a proposed iron(III)-hydroxide intermediate in iron-2OG enzymes.

ation.[24] The divergence in reactivity and lack of spectroscopic information about the iron(III)-hydroxo intermediate leads us to suggest that noncovalent interactions with the ferric-hydroxide may dictate some part of the differing reactivity observed within iron-2OG enzymes.

The few reports of synthetic iron(III)-hydroxo complexes have mostly required the presence of hydrogen bond donors in the secondary coordination sphere to stabilize the complex,[25−35] and none of these systems have mimicked the C−O(H) bond formation step common in iron-2OG enzymes. Goldberg, however, has recently reported iron(III)-methoxide and iron(IV)-hydroxo complexes that demonstrated radical rebound-like reactions with the addition of trityl-based C-centered radicals.[36,37]

Our group has previously reported the tripodal, tetradentate ligand, tris(5-cyclohexyliminopyrrol-2-ylmethyl)amine (N-(pi^{Cy})$_3$) (Scheme 1a), that binds first-row transition metal ions (M = Mn, Fe, Co, Zn), and features a secondary coordination sphere that interacts with an axial ligand bound to the metal center.[38−40] The arms of the ligand are capable of tautomerizing from the pyrrole-imine (pi) tautomeric form to the azafulvene-amine (afa) tautomeric form (Scheme 1c). Moreover, this tautomerization allows for versatility in the primary coordination sphere of the ligand (from anionic to neutral) and the noncovalent interactions imparted by the secondary coordination sphere (hydrogen bond accepting or donating).

Inspired by the work of the Chang[27] and Goldberg[41−43] groups, who have used polypyridyl ligands with a secondary coordination sphere to study high-valent iron chemistry, we sought to combine the polypyridyl system with the tautomerizable pyrrole-imine motif into a single ligand scaffold. Herein, we report the synthesis of a tetrapodal, pentadentate ligand, 2,2′,2′-methylbis-pyridyl-6-(2,2′,2′-methylbis-5-cyclohexyliminopyrrol)-pyridine, $Py_2Py(pi^{Cy})_2$, which features two of the pyrrole-imine arms previously described (Scheme 1b).[44,45] The ligand was complexed with iron(II) salts, and the synthesis and characterization of five iron complexes are reported, including two unique iron(III)-hydroxo complexes with differentiated electronic structures and reactivity analogous to iron-2OG enzymatic systems.

Scheme 1. a) Tripodal Ligand N(pi^{Cy})$_3$ Reported in Prior Studies, b) Tetrapodal Ligand Reported in This Study, and c) Ligand Arm Tautomerization

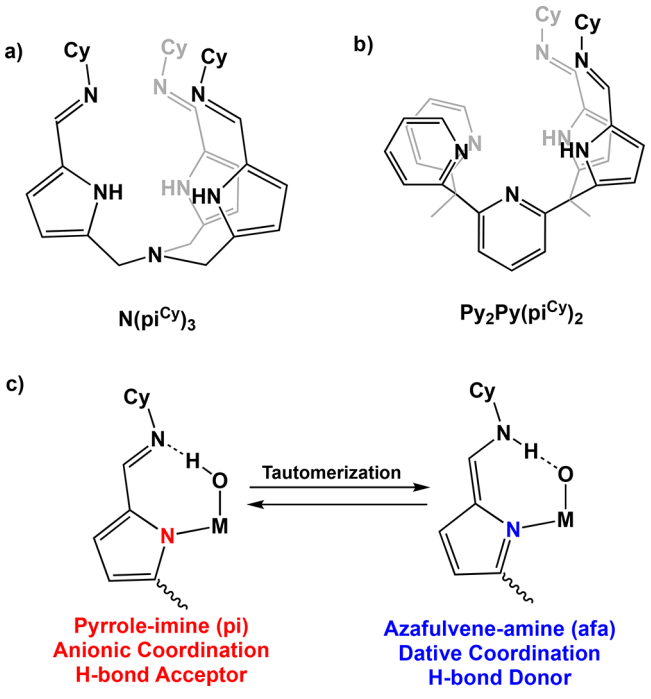

RESULTS AND DISCUSSION

Synthesis of $Py_2Py(pi^{Cy})_2$. The synthesis of 1,1-dipyridylethane was achieved from the reaction of 2-ethylpyridine and ^{n}butyllithium, followed by the addition of half an equivalent of 2-fluoropyridine. Next, the deprotonated 1,1-dipyridyl was combined with 2-bromo-6-(1,3-dioxylane)pyridine in tetrahydrofuran, with the solvent being refluxed for 36 h to furnish **L1.** The deprotection of **L1** with aqueous 3 M HCl yielded **L2**, which was further functionalized through the installation of two pyrrole functionalities (**L3**). Formylation at the 5' position of the pyrrole moieties was accomplished through a Vilsmeier−Haack reaction (**L4**), and the subsequent condensation with cyclohexylamine produced the desired ligand, $Py_2Py(pi^{Cy})_2$ in good yields (Scheme 2).

Synthesis of Iron(II) Complexes. $Py_2Py(pi^{Cy})_2$ was dissolved in tetrahydrofuran to form a pale yellow solution to which $Fe(OTf)_2(MeCN)_2$ (OTf = trifluoromethanesulfonate) was added. An immediate color change to deep red was observed, followed by the precipitation of a yellow solid. After 1 h of stirring, the suspension was filtered and the yellow precipitate, $[Py_2Py(afa^{Cy})_2Fe^{II}OTf](OTf)$ (**1**), was isolated (Figure 2). Characterization of this compound by IR spectroscopy revealed tautomerization of the pyrrole-imine moieties of the free ligand to the azafulvene-amine tautomeric form, with a C=N stretch at 1635 cm^{-1} (Figure S11 of the Supporting Information, SI); the same was reported for the corresponding iron(II) complex of the tripodal ligand system,

DOI: 10.1021/jacs.9b01516
J. Am. Chem. Soc. XXXX, XXX, XXX−XXX

Scheme 2. Synthesis of $Py_2Py(pi^{Cy})_2$[a]

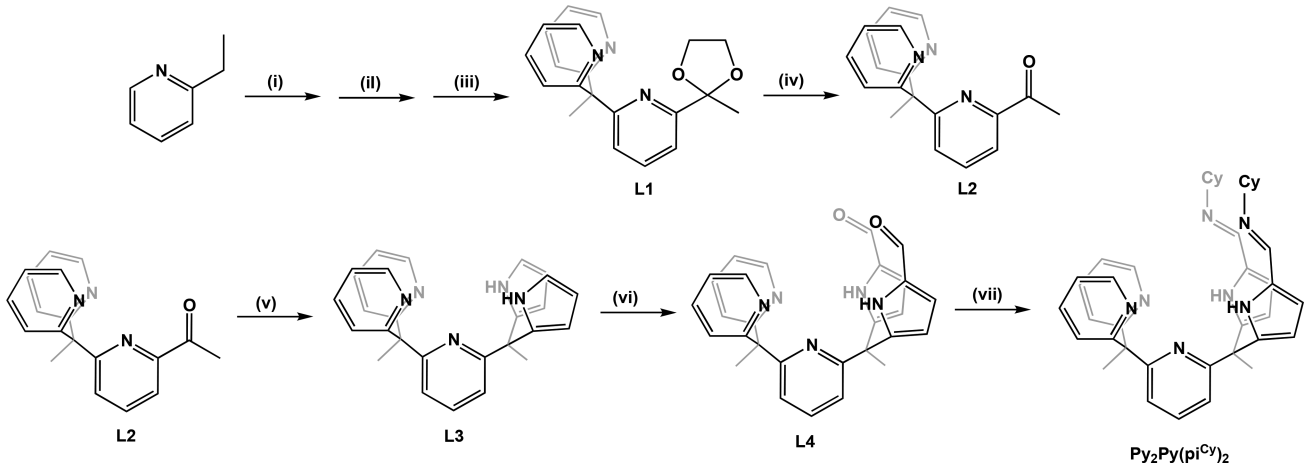

[a](i) ^{n}BuLi (1.6 M in hexanes), THF, 0.5 h, −78 °C (ii) 0.5 equiv 2-fluoropyridine, −20 °C to reflux, 1 h (iii) 0.4 equiv 2-bromo-6-(1,3-dioxylane)pyridine, 36 h, THF, reflux (iv) 3 M HCl, 4 h, rt (v) excess pyrrole, 3 M HCl, THF, 18 h (vi) 2.1 equiv $POCl_3$, DMF/DCM, 2 h, $NaOAc/H_2O$, 45 °C, 1 h (vii) 2.1 equiv cyclohexylamine, DCM, 18 h. See the Experimental Section for full details and characterization.

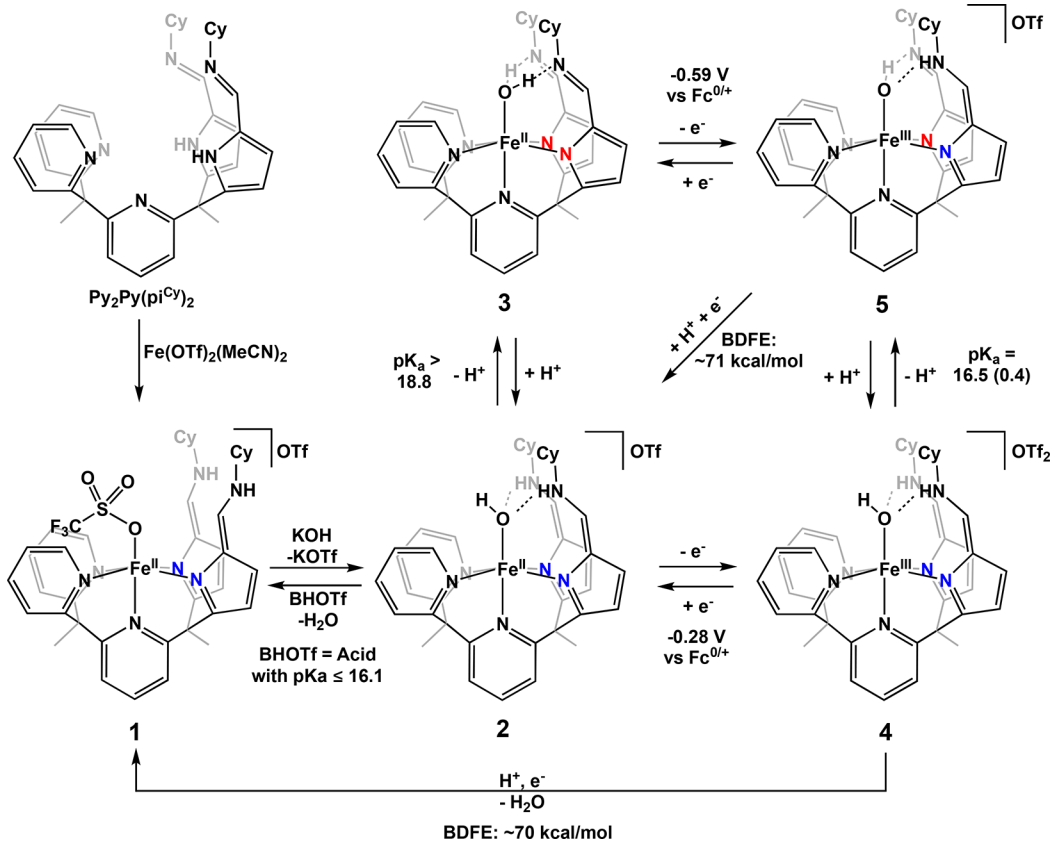

Figure 2. Complexation of $Py_2Py(pi^{Cy})_2$ and interconversion between iron complexes. All pK_a and reduction potential values are reported in acetonitrile.

$N(afa^{Cy})_3Fe^{II}OTf_2$).[38] Stretches observed at 3215 and 3285 cm^{-1} were assigned as N−H stretches of the amines. Crystals suitable for X-ray diffraction were grown from vapor diffusion of diethyl ether into a concentrated solution of **1** in acetonitrile. Refinement of the data revealed an octahedral iron(II) center coordinated to three pyridyl nitrogen atoms, two azafulvene nitrogen atoms, and one oxygen atom of a triflate anion (Figure 3). Both of the amine moieties of the secondary coordination sphere were pointed away from the iron center, with one amine engaged in hydrogen bonding to the outer-sphere triflate.

To determine if the ligand arms were able to hydrogen bond with a bound axial ligand, **1** was reacted with KOH in acetonitrile, turning the yellow solution bright red over the course of 1 h. After the removal of solvent in vacuo, the residue was treated with dichloromethane to solubilize the desired metal species. Analysis of the red product, $[Py_2Py(afa^{Cy})_2Fe^{II}OH]OTf$ (**2**), by IR spectroscopy showed a C═

DOI: 10.1021/jacs.9b01516
J. Am. Chem. Soc. XXXX, XXX, XXX−XXX

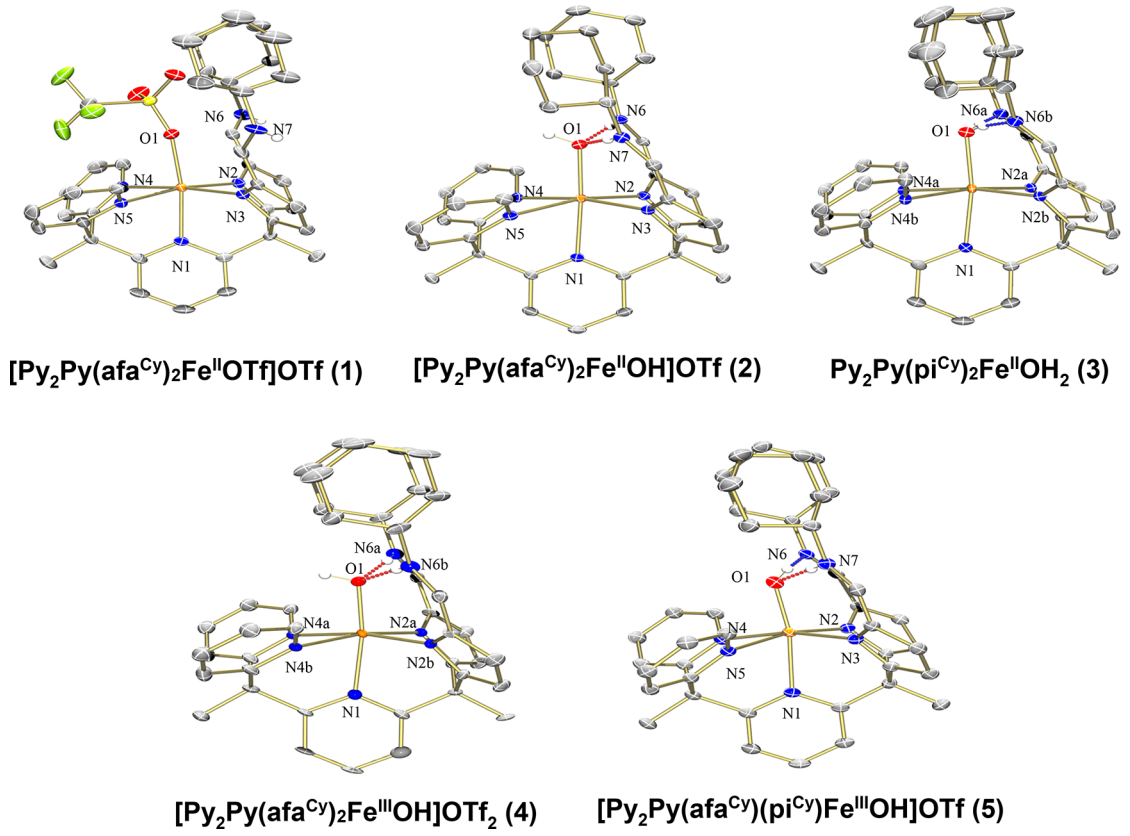

Figure 3. Structural characterization of complexes **1**−**5**. Complexes **3** and **4** contained half of the target molecule in the unit cell with the other half being symmetry generated. Non-hydrogen bonding hydrogen atoms, anions, and solvent molecules have been omitted for clarity.

Table 1. Selected Bond Distances (Å), Angles (°), and IR Data of Iron(II) and Iron(III) Complexes, 1−5

	1	2	3	4	5
Fe−O_1	2.2035(18)	2.0020(12)	2.0954(17)	1.861(8)	1.8755(18)
Fe−N_1	2.2078(19)	2.2531(14)	2.218(2)	2.211(10)	2.245(2)
Fe−N_{afa}	2.1313(19)	2.1498(15)		2.074(7)	2.106(2)
Fe−N_{afa}	2.1313(19)	2.1639(14)			
Fe−N_{pi}			2.1394(14)		2.066(2)
Fe−$py_{(4/5)}$(avg)	2.186(2)	2.2238(14)	2.2095(14)	2.183(7)	2.201(2)
N_{afa}(H)---O (avg)		2.6853		2.769	2.670(3)
N_{pi}---(H)O (avg)			2.7490(16)		2.747(3)
Fe−O−$N_{6/7}$(avg)		102.72	99.77	104.72	103.66
$\nu_{C=N}$(cm^{-1})	1635	1656	1615	1660	1616, 1658
ν_{O-H}or ν_{N-H}(cm^{-1})	3215, 3285	3640		3585	

N stretch at 1656 cm^{-1}, consistent with the azafulvene−amine tautomeric form of the ligand, and a feature at 3640 cm^{-1}, assigned as an O−H stretch (Figure S13). Crystals suitable for X-ray diffraction were grown from the vapor diffusion of diethyl ether into a concentrated solution of **2** in acetonitrile. Analysis of the data showed a hydroxo ligand bound to the iron center (Figure 3). Both azafulvene-amine arms of the secondary coordination sphere were engaged in hydrogen bonding to the hydroxo ligand with distances of 2.6666(18) and 2.7040(19) Å between the O and N_{afa} hydrogen bond donor (Table 1). The Fe−O distance of 2.0020(12) Å is similar to reported iron(II)-hydroxo complexes.[26,27,38,46−49] The solution magnetic moment (μ_{eff}) of 5.21 μ_B was determined by Evans' method, corroborating the assignment of **2** as a high spin S = 2 iron(II) species.

It was determined that **2** could be converted back to **1** through the addition of 2-aminobenzimidazolium triflate (pK_a = 16.1 in acetonitrile)[50] to form what we tentatively assign as an iron(II)-aquo species (Figure S25); subsequent release of water reforms **1** upon removal of volatiles or attempts at crystallization (Figure 2). Alternatively, the addition of benzylammonium triflate (pK_a = 16.9 in acetonitrile) showed no reactivity toward **2**, as assayed by ^{1}H NMR spectroscopy (Figure S26). The observed reactivity led to the assignment of a lower limit pK_b value of 16.1 for **2** (the exact pK_b may be slightly different due to ligand exchange energetics between the loss of water and triflate binding to the iron).

We were also interested in investigating both the acidity of **2** and the possibility of anionic coordination of the ligand to the iron center. The addition of 1 equiv of KH to **2** in acetonitrile led to the formation of a bright pink precipitate identified as

DOI: 10.1021/jacs.9b01516
J. Am. Chem. Soc. XXXX, XXX, XXX−XXX

$Py_2Py(pi^{Cy})_2Fe^{II}OH_2$ (**3**). The pK_a of **2** was determined through the addition of bases with reported pK_a values in acetonitrile[50] and monitoring the solution for the precipitation of **3**. It was determined that triethylamine (pK_a = 18.82) could not deprotonate **2** (Figure S27), while addition of pyrrolidine (pK_a = 19.56) led to the precipitation of **3**, establishing a lower bound for the pK_a for **2**. Complex **3** could also be protonated with 2,6-lutidinium triflate (LuHOTf) to reform **2** (Figure 2).

Further characterization of **3** was achieved with IR spectroscopy, displaying a single C═N stretch in the IR spectrum at 1615 cm^{-1} (Figure S14), consistent with previously reported values of anionic coordination of the pyrrole-imine tautomeric form.[38] Crystals suitable for X-ray diffraction were grown from vapor diffusion of diethyl ether into a concentrated solution of **3** in a 5:1 mixture of dimethylacetamide and dichloromethane. The resulting structure showed an iron(II)-aquo complex, with an Fe−O bond length of 2.0954(17) Å (Figure 3).

Synthesis of Iron(III) Complexes. With the iron(II) complexes in hand, the oxidations of **2** and **3** to their corresponding ferric species were investigated (Figure 2). Silver triflate (AgOTf) was added to a solution of **2** in dichloromethane in the dark, turning the bright red solution dark red-brown immediately. Filtration of the solution revealed the presence of Ag^0, and upon evaporation of the filtrate, a brown residue was obtained. Analysis of the product by IR spectroscopy showed a C═N stretching frequency at 1660 cm^{-1} (Figure S16), confirming the azafulvene-amine tautomeric form of the ligand. There was also a broad stretch observed at 3585 cm^{-1} that we tentatively assign as an O−H stretch. Crystals suitable for X-ray diffraction were grown from the vapor diffusion of diethyl ether into a concentrated solution of the metal complex in acetonitrile. Refinement of the data revealed an iron(III)-hydroxo species, $[Py_2Py(afa^{Cy})_2Fe^{III}OH](OTf_2)$ (**4**), isostructural to **2**, with a contraction of the Fe−O bond to 1.861(8) Å and the presence of a second outer-sphere triflate anion (Figure 3). The solution magnetic moment of **4** was determined by the Evans method to be 6.11(26) μ_B, consistent with a high spin S = 5/2 iron(III) center.[26,32,51,52]

Similarly, a pink suspension of **3** in dichloromethane was oxidized in the presence of AgOTf, forming a red-brown solution. Analysis of the product by ^{1}H NMR spectroscopy yielded a similar spectrum to **4** (Figure S17); however, a new resonance at 22 ppm and changes in the broad resonances between 60 and 120 ppm suggested the formation of a new species. IR spectroscopy showcased the presence of both the pyrrole-imine and azafulvene-amine tautomers, with C═N stretches at 1616 and 1658 cm^{-1}, respectively (Figure S18). Crystals suitable for X-ray diffraction were grown from the vapor diffusion of diethyl ether into a concentrated solution of the metal complex in dichloromethane. Refinement of the data revealed another iron(III)-hydroxo complex, $[Py_2Py(afa^{Cy})(pi^{Cy})Fe^{III}OH]OTf$ (**5**), that contained one outer-sphere triflate anion and the presence of a hydroxo ligand bound to the iron. The hydroxo proton was acting as a hydrogen bond donor to a pyrrole-imine ligand arm, with the other ligand arm in the azafulvene-amine tautomer donating a hydrogen bond to the hydroxo moiety. (Figure 3). The Fe−O bond length of **5** (1.8755(18) Å) is similar to **4**, which was also assigned as an iron(III)-hydroxo and contracted relative to **2**. The solution magnetic moment of **5** was 5.97(14) μ_B, supporting its formulation as a high spin S = 5/2 iron(III) center.

Furthermore, the interconversion of the ferric hydroxide complexes was achieved by the addition of LuHOTf to **5** or KH to **4**. The pK_a of **4** was determined through the addition of bases with reported pK_a values in acetonitrile[50] and monitoring the solution by ^{1}H NMR spectroscopy for the formation of **5**. It was determined that benzylamine (pK_a = 16.91) could deprotonate **4** while 2-aminobenzimidazole (pK_a = 16.08) could not (Figure S28 and S29), giving an estimated pK_a of 16.5 (±0.4) (Figure 2).

Characterization of Electronic Structure. The electronic structures of the iron complexes were investigated using Mössbauer spectroscopy. The 6 K Mössbauer spectra of polycrystalline powders of compounds **1**−**3** show quadrupole doublets (Figure 4) with isomer shifts between 1.10 and 1.15 mm/s and large quadrupole splittings (ΔE_Q > 1.90 mm/s) typical for high spin ferrous complexes with N/O coordination.[53] As is typical for molecular complexes in polycrystalline samples, the electronic spin relaxes quickly on the Mössbauer time-scale, therefore no hyperfine structure is observed. The asymmetric broadening of doublets **1** and **2** is consistent with anisotropic spin relaxation effects and it is not observed at higher temperatures (>100 K) or in zero field (spectrum of complex **3**). In contrast to **1**−**3**, complexes **4** and **5** exhibit paramagnetic spectra at 6 K. The isomer shifts of 0.5 mm/s and small quadrupole splittings are typical for S = 5/2 ground states, as are the spectral patterns (Table S1).

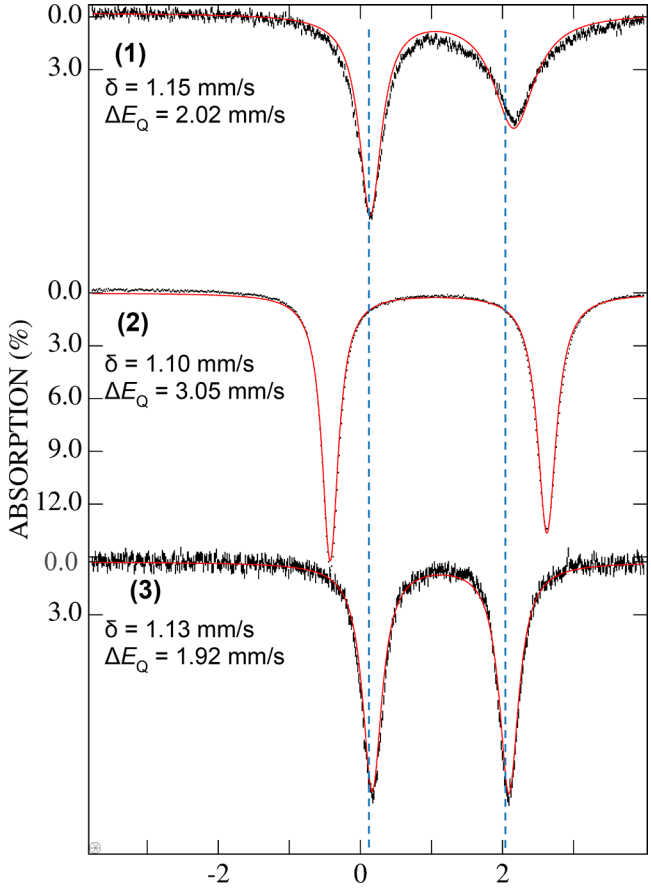

Figure 4. Mössbauer spectra of complexes **1**−**3** at 6 K and 70 mT for (1) and (2) and in 0 T (3). Hash marks are raw data, red lines are spectral simulations with the parameters shown. Full simulation parameters are located in the SI.

DOI: 10.1021/jacs.9b01516
J. Am. Chem. Soc. XXXX, XXX, XXX−XXX

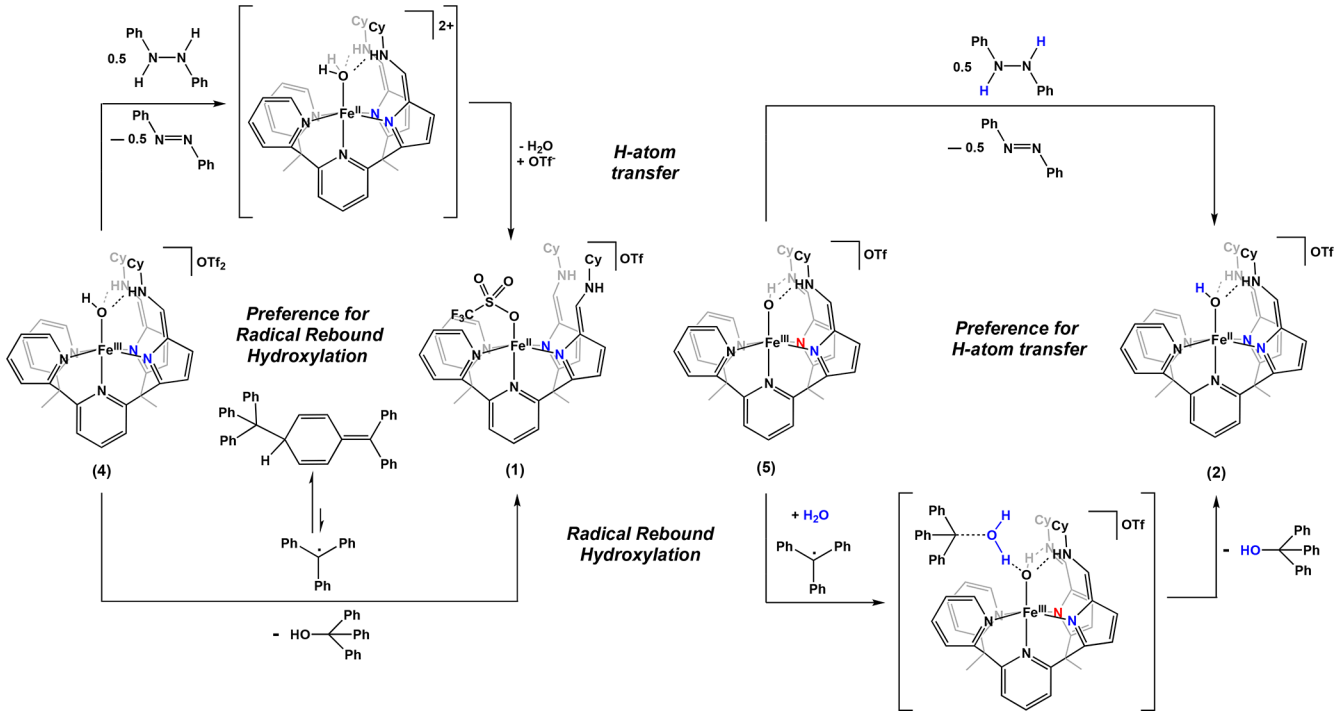

Figure 5. Preference in reactivities between complexes **4** and **5**. Complex **4** performs radical rebound hydroxylation at a faster rate then H atom transfer for selected substrates. Complex **5** will not perform radical rebound hydroxylation unless in the presence of opportunistic water, while readily performing an H atom transfer reaction.

Complexes **4** and **5** were further differentiated using X-band EPR spectroscopy at 10 K. The spectra are complex and not easily simulated, but they illustrate the differentiated electronic structures for each ferric hydroxo species (Figure S24). Further characterization of the electronic structures of this series of iron complexes is ongoing due to the complexities of the Mössbauer and EPR spectra.

Reduction of Iron(III) Complexes. The reversibility of the iron redox events was examined using cyclic voltammetry (Figure S23) and chemical reductants. The cyclic voltammograms showed the reversible reduction of **4** to **2** and **5** to **3** with the reduction potential of **5** nearly 300 mV more positive than that of **4** (Figure 2). The chemical reductions of the iron(III)-hydroxo complexes, **4** and **5** in acetonitrile, were also investigated. Addition of cobaltocene (Cp_2Co, $E^0 = -1.33$ V vs $Fc^{0/+}$) to **4** and **5** produced the corresponding iron(II) products, **3** from **5**, in good yields (99% and 78%, respectively).

H-Atom Transfer to Iron(III)-Hydroxo Complexes. One other synthetic iron(III)-hydroxo has been reported to perform HAA using 1-hydroxy-2,2,6,6-tetramethylpiperidine (TEMPO-H, BDFE = 66.5 kcal/mol) to form a ferrous-aquo species, analogous to dehydration reactions observed in some nonheme iron enzymes.[54] Determination of the iron(II)/iron(III) redox couples and the pK_a values (Figure 2) allowed for an estimation of the bond dissociation free energies (BDFEs) of the iron complexes using eq 1.[55] Due to the complicating nonequilibrium effects in the pK_a determination of **2** (precipitation of **3** in acetonitrile), the reduction potential between **2** and **4** and the pK_a between **4** and **5** were used in the BDFE calculation of **2**, which was determined to be approximately 71 kcal/mol. Similarly, a BDFE of ~70 kcal/mol was determined for **1** using the reduction potential between **2** and **4** and the pK_a between **2** and **1** (the exact BDFE may be slightly different due to the ligand exchange energetics going between complexes). These data show that **4** and **5** have similar driving forces for the oxidation of substrates with BDFEs falling between the iron(IV)-oxo (87 kcal/mol) and iron(III)-oxo (66 kcal/mol) complexes reported by Borovik.[51,56]

$$\mathrm{BDFE}_{(\mathrm{O-H})} = 23.06E_{1/2} + 1.37\mathrm{p}K_a + C$$
$$C = 54.9 \text{ kcal/mol in acetonitrile} \quad (1)$$

To assay the calculated BDFEs experimentally, 1,2-diphenylhydrazine (DPH, BDFE = 69 kcal/mol) was used as an H-atom transfer source. The addition of DPH to **5** in acetonitrile resulted in a color change from dark brown-red to bright red over the course of 1 h (Figure 5, top right). The formation of azobenzene was noted and **2** was identified as the only product by ^{1}H NMR spectroscopy (Figure S35). Similarly, the addition of DPH to **4** resulted in the formation of the proposed iron(II)-aquo intermediate, before loss of water resulted in the formation of **1** (Figure 5, top left). The rates of the reactions were also surveyed under pseudo-first order conditions using time-resolved UV−visible spectroscopy (Figures S44 and S45).

Interestingly, the addition of weak C−H bonds such as 1,4-cyclohexadiene or dihydroanthracene (BDFEs ~77 kcal/mol in acetonitrile) resulted in no reaction for either complex (Figures S37 and S38). Since complexes **4** and **5** are unable to activate even weak C−H bonds, these species may provide important mechanistic insights concerningiron-2OG desaturase enzymes.

The desaturation of C−C bonds is most commonly observed in heme and di-iron enzymes that maintain an iron(IV) species after the first HAA from substrate.[57] By comparison, iron-2OG enzymes do not seem as well-equipped

DOI: 10.1021/jacs.9b01516
J. Am. Chem. Soc. XXXX, XXX, XXX−XXX

to perform a second HAA with the formation of an iron(III)-hydroxo, instead of a more oxidatively potent iron(IV) species. However, multiple iron-2OG enzymes have demonstrated the installation of olefins, with most studies invoking a mechanism of two subsequent HAAs.[22,58,59] A recent mechanistic investigation for one of these desaturases highlighted the importance a heteroatom (N or O) adjacent to the desaturation site for most native substrates in iron-2OG enzymes.[20] The heteroatom is proposed to assist in the removal of the second H-atom through a polar cleavage mechanism (electron transfer-proton transfer), as opposed to a concerted HAA by the iron(III)-hydroxo.

The same study, and others[60,61] have shown that substrates without the presence of a heteroatom can also be desaturated by iron-2OG enzymes. Not all reports of iron-2OG desaturation enzymes have detailed product profiles, so it is difficult to know if substrate hydroxylation overrides or is in close competition with desaturation in all iron-2OG enzymes. However, the inability of **4** and **5** to react with weak C−H bonds supports the observation that a second HAA may not be operative in all desaturation mechanisms for iron-2OG desaturase enzymes due to the iron(III)-hydroxo intermediate's lack of oxidizing power. It is possible that the C−H bond involved in the second H atom removal (proximal to the C· from the first HAA) is significantly weakened to the point where the iron(III)-hydroxo could abstract an H atom, but we are not aware of studies that identify the extent to which that C−H bond is weakened.

Hydroxylation of Gomberg's Dimer. In addition to exploring the oxidative potency of **4** and **5**, we sought to determine if a radical rebound hydroxylation could be accomplished by the iron(III)-hydroxide complexes.

The addition of 0.5 equiv of Gomberg's dimer to **4** at room temperature led to a rapid color change from dark brown-red to yellow. Analysis of the organic species in the reaction showed production of triphenylmethanol in high yield (99% by GC−MS with mesitylene internal standard, Figure S31). The hydroxylation of the triphenylmethylradical species was concomitant with the formation of **1** (83% crystalline yield, Figure 5, bottom left). This reaction represents a rare example of radical rebound hydroxylation with an iron(III)-hydroxo.

The rate of hydroxylation was investigated further using UV−visible spectroscopy. The stoichiometric reaction of **4** reacting with Gomberg's dimer was completed within a minute with isosbestic conversion to **1** (Figure S40). Under pseudo-first order conditions with 10 equiv of Gomberg's dimer, the hydroxylation was complete within approximately 10 s at 25 °C (Figure S41). Additionally, an ^{18}O isotopologue of **4** was synthesized from **1** with the use of $H_2{}^{18}O$, and incorporation up to 71% was observed for the ^{18}O isotopologue of **4** (Figure S46, Table S2). We hypothesize the actual isotope incorporation is higher due to a larger percentage incorporation of the ^{18}O label into triphenylmethanol (82%, Figure S49, Table S5) from the reaction of the ^{18}O isotopologue of **4** with triphenylmethyl radical. The observed differences suggest there may be some exchange with adventitious water and the hydroxo ligand of **4** prior to analysis of the metal complexes by ESI−MS. The exchange of water and the hydroxo ligand was corroborated by stirring unlabeled **4** in acetonitrile spiked with $H_2{}^{18}O$ for 1 h, leading to ∼50% incorporation of ^{18}O label in complex **4** (Figure S48, Table S4).

Attempts to determine if the hydroxyl ligand is concertedly transferred to substrate through the use of para-substituted trityl derivatives were inconclusive due to incompatible solvents for the production of the monomeric trityl radical derivatives and solubility of **4**. A future study modifying the ligand scaffold, as has previously been demonstrated,[49] should allow for discrimination between a concerted hydroxyl transfer mechanism or an electron-transfer cation-transfer (ET-CT) pathway.

To contrast the differences between the two ferric-hydroxide complexes, Gomberg's dimer was added to **5** to determine if it was also capable of performing the hydroxylation reaction that is dominant in most iron-2OG enzymes. Over the course of 24 h the reaction mixture turned from dark red-brown to bright red. Analysis of the reaction by ^1H NMR spectroscopy showed the formation of **2**, with partial consumption of Gomberg's dimer to form triphenylmethanol over 24 h (Figure S34). The sluggish rate of the reaction and the formation of **2** (a net H-atom transfer) suggest that the hydroxylation of Gomberg's dimer cannot be accomplished by **5** alone.

We hypothesized that adventitious water interacts with **5** and the triphenylmethylradical to perform the small amount of hydroxylation that is observed (Figure 5, bottom right). To test this, the reaction of **5** and Gomberg's dimer was performed in solvent spiked with $H_2{}^{18}O$. The conversion of **5** to **2** was observed over the course of 1 h, and analysis of the triphenylmethanol by EI−MS showed 72% incorporation of the ^{18}O label into the substrate (Figure S46, Table S3), leading to the proposed intermediate shown in Figure 5. Alternatively, an ^{18}O isotopologue of **5** was synthesized from $H_2{}^{18}O$ and reacted in dry solvent for 24 h. Not enough triphenylmethanol was formed from the reaction to determine the amount of isotope label that was incorporated, showing the need for adventitious water for the hydroxylation reaction to occur.

Monitoring the ^1H NMR spectrum of **5** showed no change in the paramagnetic resonances upon addition of H_2O; however, upon addition of Gomberg's dimer to this solution, conversion to **2** was observed (Figure S39). Similarly, the reaction of **5** and Gomberg's dimer in wet solvent under pseudo-first order conditions was monitored by UV−visible spectroscopy, and showed the reaction proceeding to completion within 10 min (Figure S43). Monitoring the reaction in dry solvent did show some consumption of the triphenylmethylradical, but only minimal conversion was observed (Figure S42).

We propose that the noncovalent interactions from the ligand have a profound effect on regulating the hydroxylation reactivity of complexes **4** and **5** and could be representative of noncovalent interactions observed in iron-2OG enzymes. Since the proposed iron(III)-hydroxo intermediate has not been observed in iron-2OG enzymes, an analysis of the residues surrounding the iron active site, and subsequent mutagenesis studies, may lend insight into how desaturase enzymes bias their reactivity from hydroxylation to desaturation. Our data suggest the engagement of the hydroxo ligand with a hydrogen bond acceptor in the secondary coordination sphere may play a role in deterring the rebound hydroxylation pathway observed in most iron-2OG enzymes. Further kinetic studies will need to be conducted on our system to determine the effect of reduction potential on hydroxylation reactivity, as well as assigning a concerted hydroxylation mechanism or an ET-CT mechanism.

DOI: 10.1021/jacs.9b01516
J. Am. Chem. Soc. XXXX, XXX, XXX−XXX

CONCLUSIONS

The synthesis and characterization of five iron complexes, including two differentiated ferric hydroxo complexes, was accomplished. Interestingly, both iron(III)-hydroxo complexes exhibited BDFEs incapable of abstracting an H atom from even weak C−H bonds. These data support recent observations in iron-2OG desaturase enzymes that go through a polar-cleavage mechanism instead of a second HAA to desaturate substrates. The two ferric hydroxo complexes showed differing reactivity toward the hydroxylation of radical substrate, with **5** not performing hydroxylation without the presence of water. We attribute the differences in reactivity to the presence of an H-bond acceptor interacting with the hydroxo ligand and the lesser oxidizing reduction potential of **5**. It is plausible that iron-2OG desaturase enzymes are also able to tune the metal reduction potential or employ H-bond acceptors proximal to the metal active site to help bias the enzyme toward substrate desaturation and away from hydroxylation.

EXPERIMENTAL SECTION

General Considerations. All manipulations of air- and moisture-sensitive metal compounds were carried out in the absence of water and dioxygen using a MBraun inert atmosphere drybox under a dinitrogen atmosphere. All glassware was oven-dried for a minimum of 8 h and cooled in an evacuated antechamber prior to use in the drybox. Solvents were dried and deoxygenated on a Glass Contour System (SG Water U.S.A., Nashua, NH) and stored over 4 Å molecular sieves (3 Å in the case of acetonitrile) purchased from Strem prior to use. Chloroform-d_1, dichloromethane-d_2, and acetonitrile-d_3 were purchased from Cambridge Isotope Laboratories and stored over 4 Å molecular sieves prior to use. 2,6-dibromopyridine (Oakwood Chemical), ^{n}butyllithium (1.6 M in hexanes) (Sigma-Aldrich), dimethylacetamide (Sigma-Aldrich), ethylene glycol (Macron), *p*-TSA·H_2O (Sigma-Aldrich), 2-fluoropyridine (Oakwood Chemical), pyrrole (Sigma-Aldrich), $POCl_3$ (Sigma-Aldrich), cyclohexylamine (Oakwood Chemical), lithium oxide (Sigma-Aldrich), silver triflate (Strem), potassium hydride (Sigma-Aldrich), triflic acid (Sigma-Aldrich), potassium hydroxide (Fischer Scientific), 2,6-lutidine (Sigma-Aldrich), triethylamine (Sigma-Aldrich), 2-aminobenzimidazole (Sigma-Aldrich), pyrrolidine (Sigma-Aldrich), benzylamine (Sigma-Aldrich), 1,8-diazabicyclo[5.4.0]undec-7-ene (Sigma-Aldrich), and $H_2{}^{18}O$ (97% enrichment, Sigma-Aldrich) were purchased from the vendor listed and used as received. Diphenylhydrazine (Sigma-Aldrich) was recrystallized from a mixture of diethyl ether and hexanes at −35 °C. $Fe(OTf)_2(MeCN)_2$,[62] LuHOTf,[63] and Gomberg's[37] dimer were prepared according to modified literature procedures. Ligand precursors 6-bromo-2-acetylpyridine[64] and 2-bromo-6-(1,3-dioxylane)pyridine[64] were synthesized according to literature procedures and identified by their ^{1}H NMR spectra. Celite 545 (J.T. Baker) and tetrabutylammonium hexafluorophosphate ($[nBu_4N][PF_6]$) (Sigma- Aldrich) were dried in Schlenk flasks for 24 h under a dynamic vacuum while heating to at least 150 °C prior to use in a drybox.

Physical Measurements. NMR spectra for ligand precursors were recorded on a Varian spectrometer operating at 400 MHz (^{1}H NMR) or a Bruker spectrometer operating at 500 MHz (^{1}H NMR) or 126 MHz (^{13}C NMR). NMR spectra of metal complexes were recorded on a Varian spectrometer at 500 MHz (^{1}H NMR) or 377 MHz (^{19}F NMR). All ^{1}H and ^{13}C chemical shifts (ppm) are reported relative to the resonance of the residual solvent; ^{19}F chemical shifts are reported relative to an external standard (1% $CFCl_3$ in $CDCl_3$). Solid-state infrared spectra were recorded using a PerkinElmer Frontier FT−IR spectrophotometer equipped with a KRS5 thallium bromide/iodide universal attenuated total reflectance accessory. UV−visible spectra were recorded on an Agilent 8453 Spectrophotometer with accompanying software. All samples were prepared in a drybox containing a dinitrogen atmosphere in quartz cuvettes with a 1 cm path length and capped with a rubber septum. Elemental analyses were performed by the University of Illinois at Urbana−Champaign School of Chemical Sciences Microanalysis Laboratory in Urbana, IL. Samples submitted for elemental analyses were dried under vacuum for a minimum of 12 h; solvates were confirmed by ^{1}H NMR spectroscopy. Mass spectra were recorded by the University of Illinois mass spectroscopy laboratory.

Electrochemical experiments were carried out using a CH Instruments CHI410C Electrochemical Workstation. The supporting electrolyte was 0.1 M $[^nBu_4N][PF_6]$ in acetonitrile. A glassy carbon working electrode, a platinum wire counter electrode, and a silver wire pseudoreference electrode were used. The concentration of each analyte was 1 mM. Experiments were performed at a scan rate of 100 mV/s. Each scan was referenced to internal $Fc^{0/+}$. EPR samples were prepared in an MBraun glovebox under a dinitrogen atmosphere. The sample concentration was 5 mM in 1:1 acetonitrile/dichloromethane. EPR spectra were recorded on a Varian E-line 12′′ Century series X-band CW spectrometer, and the spectra were simulated using the program SIMPOW6.3. Analysis by Gas Chromatography Mass Spectrometry (GC−MS) was performed using a Shimadzu GC-2010 Plus Gas Chromatograph equipped with a Shimadzu GCMS-QP2010 SE mass spectrometer using electron impact ionization (EI) after traveling through a SH-RxiTM-5 ms 30 m × 0.32 mm × 0.25 μm column with helium carrier gas. Zero and low-field (0.07 T), variable-temperature (5−200 K) Mössbauer spectra were recorded on a closed-cycle refrigerator spectrometer, model CCR4K (SeeCo, Edina, MN) equipped with a 0.07 T permanent magnet, maintaining temperatures between 5 and 300 K. The samples consisted of solid powders (or crystalline material) suspended in Icosane placed in Delrin 1.00 mL cups, and frozen in liquid nitrogen. The isomer shifts are quoted at 5 K with respect to iron metal standard at 298 K. Mössbauer spectra were analyzed using the software WMOSS4 (Ion Prisecaru, www.wmoss.org).

2,2′,2′-Methylbis-pyridyl-6-(2-methyl-1,3-dioxolan-2-yl)-pyridine (L1). L1 was synthesized using a modified literature procedure.[65] To a 250 mL three neck Schlenk flask outfitted with a gas inlet, reflux condenser topped with a rubber septum, and septum, were added 2-ethylpyridine (3.0 g, 28.0 mmol) and 50 mL of anhydrous tetrahydrofuran. N_2 was flowed through the reaction vessel for 5 min. The flask was cooled to −78 °C (dry ice/acetone) for 10 min prior to adding ^{n}Butyllithium in hexanes (17.5 mL of 1.6 M, 28.0 mmol) within 5 min, turning the yellow solution deep red. After 30 min, the reaction vessel temperature was raised to −20 °C, and 2-fluoropyridine (1.35 g, 14 mmol, 0.5 equiv) was added dropwise to the reaction. The solution was brought to room temperature over 20 min, then refluxed for 1 h. The solution was subsequently cooled to room temperature and 2-bromo-6-(1,3-dioxylane)pyridine (2.5 g, 10.2 mmol) was added in 10 mL of THF. The solution was then returned to reflux for 36 h. The flask was then cooled to room temperature and quenched with 25 mL of H_2O. The biphasic mixture was extracted with three 25 mL portions of ethyl acetate, with organic fractions combined and dried over Na_2SO_4. Volatiles were removed under reduced pressure leaving a brown oil that was used without further purification. ^{1}H NMR ($CDCl_3$, 500 MHz, 21 °C): δ 1.64 (s, 3H, $-CH_3$), 2.34 (s, 3H, $-CH_3$), 3.90−3.85 (m, 2H, $-CH_2$), 4.06−4.01 (m, 2H, $-CH_2$), 7.14−7.03 (m, 5H, py−CH), 7.35 (d, J = 7.7 Hz, 1H, py−C*H*), 7.62−7.52 (m, 3H, py−C*H*), 8.56 (ddd, J = 6.0, 3.6, 2.5 Hz, 2H py−C*H*). ^{13}C NMR ($CDCl_3$, 126 MHz, 21 °C): δ 24.28, 27.10, 60.19, 64.99, 108.84, 116.85, 121.09, 122.55, 123.63, 135.77, 136.37, 148.63, 159.33, 164.79, 166.20 ESI−MS: calculated $[C_{21}H_{22}N_3O_2]^+$: 348.1712, found: 348.1699.

2,2′,2′-Methyl-bis-pyridyl-6-acyl-pyridine (L2). To a 20 mL scintillation vial was added **L1** (2.8 g, 8.0 mol) and 10 mL of 3 M HCl. The reaction was allowed to stir for 4 h at room temperature. The solution was then transferred to a separatory funnel and neutralized with 20 mL of a saturated aqueous solution of $NaHCO_3$, followed by 10 mL of distilled H_2O. The aqueous layer was extracted with 3 portions of 25 mL of dichloromethane, with the organic layers combined and dried over Na_2SO_4. After removing the volatiles under reduced pressure, the product was obtained as a brown oil that was

DOI: 10.1021/jacs.9b01516
J. Am. Chem. Soc. XXXX, XXX, XXX−XXX

used without further purification (Yield, 2 steps: 2.4 g, 8.0 mmol, 78%) ^{1}H NMR ($CDCl_3$, 400 MHz, 21 °C): δ 2.37 (s, 3H, $-CH_3$), 2.52 (s, 3H, $-CH_3$), 7.12−7.06 (m, 2H, py−C*H*), 7.14 (ddd, J = 7.5, 4.8, 1.1 Hz, 2H, py−C*H*), 7.40 (dd, J = 7.9, 1.0 Hz, 1H, py−C*H*), 7.59 (tt, J = 7.6, 2.0 Hz, 3H, py−C*H*), 7.72 (t, J = 7.8 Hz, 1H, py−C*H*), 7.87 (dd, J = 7.7, 1.0 Hz, 1H, py−C*H*), 8.59 (ddd, J = 4.9, 1.9, 0.9 Hz, py−2H). ^{13}C NMR ($CDCl_3$, 126 MHz, 21 °C): δ 25.72, 27.21, 60.27, 119.07, 121.44, 123.47, 127.66, 136.08, 136.69, 148.91, 152.21, 165.05, 165.76, 200.80. IR ν_{max}: 1650 cm^{-1}, 1694 cm^{-1} (C═O). ESI−MS: calculated $[C_{19}H_{18}N_3O]^+$: 304.1450, found: 304.1459.

2,2′,2′-Methyl-bis-pyridyl-6-(2,2′,2′-methylbis-pyrrolyl)-pyridine (L3). **L2** (2.5 g, 8.2 mmol) was added to a 20 mL scintillation vial, along with 5 mL of pyrrole, 5 mL of 3 M HCl, and 2 mL of tetrahydrofuran. The solution was left to stir at room temperature for 18 h. Upon neutralization with a saturated aqueous solution of $NaHCO_3$, the biphasic mixture was extracted with dichloromethane (3 × 25 mL). Upon removal of the volatiles, diethyl ether was added to the orange oil to form yellow suspension. After stirring for 2 h, the suspension was filtered and the off-white solid, **L3**, was collected (1.86 g 4.4 mmol, 54%). ^{1}H NMR (CDCl3, 400 MHz, 21 °C): δ 2.02 (s, 3H, $-CH_3$), 2.35 (s, 3H, $-CH_3$), 5.93 (ddd, J = 3.3, 2.5, 1.6 Hz, 2H, pyrrole−C*H*), 6.04−6.00 (m, 2H, pyrrole−C*H*), 6.48 (td, J = 2.6, 1.5 Hz, 2H, pyrrole−C*H*), 6.96 (dd, J = 7.9, 0.8 Hz, 1H, py−C*H*), 7.12 (dt, J = 8.1, 1.0 Hz, 2H, py−C*H*), 7.22−7.16 (m, 3H, py−C*H*), 7.65−7.54 (m, 3H, py−C*H*), 8.65 (ddd, J = 4.9, 1.9, 1.0 Hz, 2H, py−C*H*), 9.03 (b, 2H, pyrrole N−H). ^{13}C NMR (CDCl3, 126 MHz, 21 °C): δ 27.34, 44.94, 59.96, 104.87, 107.37, 116.81, 117.98, 20.32, 21.62, 123.73, 136.35, 136.92, 137.85, 149.02, 164.16, 164.90, 165.87 ESI−MS: calculated $[C_{27}H_{26}N_5]^+$: 420.2188, found: 420.2203.

2,2′,2′-Methyl-bis-pyridyl-6-(2,2′,2′-methylbis-5-formyl-pyrrol)-pyridine (L4). To a 250 mL round-bottom flask were added **L3** (1.30 g, 3.1 mmol), 5 mL of dimethylformamide, and 30 mL of dichloromethane, forming a yellow solution. A solution of $POCl_3$ (1.0 g, 6.5 mmol, 2.1 equiv) in 10 mL of dichloromethane was added to the solution dropwise forming a pink solution that was heated to 40 °C for 2 h. An aqueous solution of sodium acetate was prepared (2.5 g in 50 mL distilled water) and added to the stirred solution and heated at 45 °C for 1 h. The biphasic mixture was then cooled and neutralized using solid Na_2CO_3, and extracted with dichloromethane (3 × 20 mL). Organic fractions were combined and dried over Na_2SO_4, followed by the removal of volatiles under reduced pressure to give a pink powder, **L4**, (1.6 g, 3.1 mmol, 99%). ^{1}H NMR ($CDCl_3$, 400 MHz, 21 °C): δ 2.03 (s, 3H, $-CH_3$), 2.39 (s, 3H, $-CH_3$), 6.04 (dd, J = 3.9, 2.4 Hz, 2H, pyrrole−C*H*), 6.80 (dd, J = 3.9, 2.4 Hz, 2H, pyrrole−C*H*), 7.03 (d, J = 7.8 Hz, 1H, py−C*H*), 7.12 (ddd, J = 7.5, 4.8, 1.1 Hz, 2H, py−C*H*), 7.15 (dt, J = 8.0, 1.1 Hz, 2H, py−C*H*), 7.57 (td, J = 7.7, 1.9 Hz, 2H, py−C*H*), 7.63 (t, J = 7.9 Hz, 1H, py−C*H*), 8.57 (ddd, J = 4.9, 2.0, 1.0 Hz, 2H, py−C*H*), 9.37 (s, 2H, −C*H*O), 9.86 (b, 2H-pyrrole−N*H*). ^{13}C NMR ($CDCl_3$, 126 MHz, 21 °C): δ 27.16, 27.28, 46.26, 60.07, 109.62, 118.32, 121.46, 122.20, 123.36, 128.31, 129.11, 132.61, 136.33, 137.67, 144.72, 148.94, 160.63, 165.56, 178.68. IR ν_{max}: 1650 cm^{-1} (C = O). ESI-MS: calculated $[C_{29}H_{26}N_5O_2]^+$: 476.2087, found: 476.2065.

2,2′,2′-Methyl-bis-pyridyl-6-(2,2′,2′-methylbis-5-cyclohexy-liminopyrrol)-pyridine ($Py_2Py(pi^{Cy})_2$). In a 20 mL scintillation vial **L4** (1.55 g, 3.0 mmol, 1 equiv) was dissolved in 10 mL of dichloromethane, followed by the addition of cyclohexylamine (0.65 g, 6.5 mmol, 2.2 equiv). The reaction was stirred at room temperature for 18 h followed by the removal of volatiles under reduced pressure, yielding a brown powder. The brown powder was taken into a dry glovebox, dissolved in dichloromethane, and stored over 4 Å molecular sieves overnight. Removal of volatiles under reduced pressure furnished a tan powder, $Py_2Py(pi^{Cy})_2$, (1.7 g, 2.7 mmol, 88%) ^{1}H NMR ($CDCl_3$, 400 MHz, 21 °C): 1.15−1.77 (m, 20H, cyclohexyl−CH_2), 1.90 (s, 3H, $-CH_3$), 2.47 (s, 3H, $-CH_3$), 3.00 (tt, J = 10.5, 4.0 Hz, 2H, cyclohexyl−C*H*), 5.91 (d, J = 3.6 Hz, 2H, pyrrole−C*H*), 6.30 (d, J = 3.6 Hz, 2H, pyrrole−C*H*), 6.86 (d, J = 7.8 Hz, 1H, py−C*H*), 7.09 (ddd, J = 7.5, 4.8, 1.1 Hz, 2H, py−C*H*), 7.16 (d, J = 7.9 Hz, 1H, py−C*H*), 7.20 (dt, J = 8.1, 1.1 Hz, 2H, py−C*H*), 7.58−7.48 (m, 3H, py−C*H*), 7.96 (s, 2H, imine−C*H*), 8.60−8.57 (m, 2H, py−C*H*), 9.67 (s, 2H, pyrrole−N*H*). ^{13}C NMR ($CDCl_3$, 126 MHz, 21 °C): 25.12, 25.83, 27.65, 29.00, 29.86, 34.83, 46.33, 60.42, 69.51, 108.12, 112.86, 118.62, 121.30, 123.74, 130.50, 136.24, 137.38, 139.81, 148.83, 148.92, 163.11, 164.75, 166.30. IR ν_{max}: 1635 cm^{-1} (C═N) ESI−MS: calculated $[C_{41}H_{48}N_7]^+$: 638.3971, found: 638.3957.

$[Py_2Py(afa^{Cy}_2)Fe^{II}OTf]OTf$ (1). To a 20 mL scintillation vial were added $Py_2Py(pi^{Cy})_2$ (0.032 g, 0.050 mmol), a stir bar, and 4 mL of tetrahydrofuran. After dissolution, $Fe(OTf)_2(MeCN)_2$ (21.8 mg, 0.050 mmol) was added to the solution. An immediate color change to red was observed, followed by the formation of a yellow precipitate over the course of 1 h. The reaction was filtered over diatomaceous earth, and the filtrate was discarded. The yellow solid collected by filtration was eluted with five, 1 mL portions of acetonitrile (or until no visible yellow solid remained on filter). Volatiles were removed under reduced pressure to give a yellow powder (0.040 g, 0.40 mmol, 81%). Crystals suitable for X-ray analysis were grown from the vapor diffusion of diethyl ether into a concentrated solution of the target molecule in acetonitrile at room temperature. Analysis for $C_{43}H_{47}F_6FeN_7O_6S_2$·MeCN (calcd., found:): C (52.33, 52.10), H (4.88, 4.68), N (10.85, 10.40). The poor solubility of the complex precluded its characterization by ^{1}H NMR spectroscopy and the determination of its solution magnetic moment by the Evans' Method. IR ν_{max}: 1635 cm^{-1} (C═N), 3215, 3283 cm^{-1} (N−H).

$[Py_2Py(afa^{Cy}_2)Fe^{II}OH]OTf$ (2) from 1. To a 20 mL scintillation vial was added **1** (0.032 g, 0.32 mmol), a stir bar, and 4 mL of acetonitrile. KOH (0.0030 g, 0.54 mmol) was added to the yellow suspension, and a red solution formed over 1 h. After the removal of volatiles under reduced pressure, the red residue was dissolved in dichloromethane and filtered over a pad of diatomaceous earth. The volatiles were again removed under reduced pressure, yielding a red powder (0.0265 g, 0.031 mmol, 95%). Crystals suitable for X-ray analysis were grown from vapor diffusion of diethyl ether into a concentrated solution of the target molecule in acetonitrile at room temperature. (0.0225 g, 0.026 mmol, 81%). ^{1}H NMR (d_3-CD_3CN, 21 °C): −5.7, −4.9, −3.8, −0.6, 0.2, 0..4, 0.7, 1.1, 1.9, 2.7, 2.9, 6.6, 24.0, 24.8, 34.3 (d), 51.2, 61.0, 65,0, 82.1 Analysis for $C_{42}H_{48}F_3FeN_7O_4S$: (calcd., found) C (58.67, 58.33), H (5.63, 5.73), N (11.40, 11.34). IR ν_{max}: 1656 cm^{-1} (C═N), 3637 cm^{-1} (O−H). μ_{eff} = 5.21(9) μ_B.

$Py_2Py(pi^{Cy}_2)Fe^{II}OH_2$ (3) from 1. To a 20 mL scintillation vial was added **1** (0.041 g, 0.041 mmol), a stir bar, and 4 mL of acetonitrile. Li_2O (0.005 mg, 0.16 mmol) was added to the solution. The solution changed from yellow to red over the course of 1 h, followed by the precipitation of a bright pink solid over the course of 18 h. The suspension was filtered, and the precipitate was washed with 1 mL of acetonitrile. The solid was eluted with dimethylacetamide (DMA). Crystals suitable for X-ray analysis were grown from the vapor diffusion of diethyl ether into a concentrated solution of the target complex in dimethylacetamide and dichloromethane at room temperature (0.0275 g, 92%). Analysis for $C_{41}H_{47}FeN_7O$·1DMA·0.5CH_2Cl_2 (calcd., found): C (65.11, 65.28), H (6.85, 6.49), and N (13.35, 12.93). The poor solubility of the complex precluded its characterization by ^{1}H NMR spectroscopy and the determination of its solution magnetic moment by the Evans' Method. IR ν_{max}: 1615 cm^{-1} (C═N).

$[Py_2Py(afa^{Cy}_2)Fe^{III}OH]OTf_2$ (4) from 2. To a 20 mL scintillation vial wrapped in black electrical tape were added **2** (0.0190 g, 0.022 mmol), 4 mL of dichloromethane, and a stir bar. AgOTf (0.0057 g, 0.022 mmol) was added to the solution and stirring was continued for 1 h. The mixture was filtered over diatomaceous earth, and the filtrate was dried under reduced pressure, producing a red-brown powder (0.0209 g, 0.021 mmol, 93%). Crystals suitable for X-ray analysis were grown from vapor diffusion of diethyl ether into a concentrated solution of dichloromethane and acetonitrile (1:1) at room temperature. Bulk purification was achieved by vapor diffusion of diethyl ether into a concentrated solution of dichloromethane (0.019 g, 0.019 mmol, 87%). Analysis for $C_{43}H_{48}F_6FeN_7O_7S_2$ (calcd., found): C (49.03, 49.27), H (4.68, 4.66), N (9.10, 9.08). ^{1}H NMR (d_3-CD_3CN, 500 MHz, 21 °C): 2.6, 8.2, 13.9, 19.0, 64.1, 72.6, 88.8, 109.0. IR ν_{max}: 1660 cm^{-1} (C═N), 3585 cm^{-1} (O−H), μ_{eff} = 6.11(26) μ_B.

DOI: 10.1021/jacs.9b01516
J. Am. Chem. Soc. XXXX, XXX, XXX−XXX

[$Py_2Py(afa^{Cy})(pi^{Cy})Fe^{III}OH$]OTf (5) from 3. To a 20 mL scintillation vial wrapped in black electrical tape was added **3** (0.0270 g, 0.031 mmol, 0.038 mmol), 4 mL of dichloromethane, and a stir bar. AgOTf (0.0098 g, 0.038 mmol) was added to the solution, which was stirred for 1 h. The mixture was filtered over diatomaceous earth, and the filtrate was dried under reduced pressure, producing a red-brown powder (0.0320 g, 0.037 mmol, 94%). Crystals suitable for X-ray analysis and bulk purification were grown from vapor diffusion of diethyl ether into a concentrated solution of dichloromethane and acetonitrile (1:1) at room temperature (0.0237 g, 0.028 mmol, 70%). Analysis for $C_{42}H_{47}F_3FeN_7O_4S{\cdot}CH_2Cl_2$ (calcd., found): C (54.73, 54.82) H (5.23, 5.23) N (10.39, 9.90). ^{1}H NMR (d_2-CD_2Cl_2, 500 MHz, 21 °C): 13.4, 20.0, 31.5, 65.6, 75.0, 82.2, 90.6. IRν_{max}: 1616, 1658 cm^{-1} (C═N), μ_{eff} = 5.97(14) μ_B.

Alternative Synthesis of 3 from 2. To a 20 mL scintillation vial were added **2** (0.0245 g, 0.30 mmmol), a stir bar, 4 mL of acetonitrile, and KH (0.0014 g, 0.035 mmol). The solution was stirred for 18 h, and formation of a pink precipitate was observed. Upon filtration, **3** was isolated (0.0151 g, 0.021 mmol, 76%).

Alternative Synthesis of 2 from 3. To a 20 mL scintillation vial were added **3** (0.0104 g, 0.015 mmol), a stir bar, 4 mL of tetrahydrofuran, and 2,6-lutidinium triflate (LuHOTf, 0.0038 g, 0.015 mmol). The solution was stirred for 1 h, changing from a pink solution to a bright red suspension. The solution was filtered, and the red solid was eluted with acetonitrile. Subsequent removal of volatiles under reduced pressure yielded a red powder, **2** (0.0069 g, 0.008 mmol, 55%).

Alternative Synthesis of 5 from 4. To a 20 mL scintillation vial were added **4** (0.0255 g, 0.026 mmol), a stir bar, 2 mL of acetonitrile, and potassium hydride (0.0011 g, 0.028 mmol). The solution was stirred for 1 h, with the color remaining dark red-brown. Volatiles were removed under reduced pressure and the product, **5**, was recrystallized from dichloromethane with slow diffusion of diethyl ether (0.0173 g, 0.020 mmol, 77%).

Alternative Synthesis of 4 from 5. To a 20 mL scintillation vial were added **5** (0.0118 g, 0.014 mmol) , a stir bar, 4 mL of dichloromethane, and 2,6-lutidinium triflate (LuHOTf, 0.0036 g, 0.014 mmol). The solution was stirred for 1 h, remaining dark red-brown in color. Volatiles were removed under reduced pressure, and the product was recrystallized from acetonitrile with slow diffusion of diethyl ether (0.0102 g, 0.010 mmol, 73%).

Alternative Synthesis of 2 from 4. To a 20 mL scintillation vial were added **4** (0.0123 g, 0.012 mmol), a stir bar, and 4 mL of acetonitrile. Cobaltocene (0.0024 g, 0.012 mmol) was added to the stirred solution and an immediate color change was noted from dark red-brown to bright red. Volatiles were removed under reduced pressure and the product was recrystallized from acetonitrile with slow diffusion of diethyl ether (0.0105 g, 0.012 mmol, > 99%).

Alternative Synthesis of 3 from 5. To a 20 mL scintillation vial were added **5** (0.0183 g, 0.021 mmol), a stir bar, and 4 mL of acetonitrile. Cobaltocene (0.0041 g, 0.021 mmol) was added to the stirred solution and the appearance of a pink precipitate over the course of 1 h was noted. Filtration of the suspension yielded the product, **3** (0.0117 g, 0.016 mmol, 78%).

Alternative Synthesis of 2 from 5. To a 20 mL scintillation vial were added 0.0129 g (0.015 mmol) of **5**, 4 mL of acetonitrile, and 0.0028 mg (0.015 mmol) of 1,2-diphenylhydrazine. The solution was stirred for 1 h, producing a bright red solution. Volatiles were removed under reduced pressure, and the resulting powder was triturated with diethyl ether. The product, **2**, was recrystallized from acetonitrile with vapor diffusion of diethyl ether (0.0079 g, 0.009 mmol, 61%).

Synthesis of ^{18}O Isotopologue of 4. Complex **1** (40 mg, 0.04 mmol) was dissolved in 2 mL of acetonitrile spiked with $H_2{}^{18}O$ (~5 mg/mL) forming an orange solution. One drop of triethylamine (~10 mg, 0.1 mmol) was added to the solution turning it bright red immediately. The solution was left to stir for 1 h and then concentrated to ~1 mL volume and the ^{18}O isotopologue of **2** was recrystallized from vapor diffusion of diethyl ether into acetonitrile. The recrystallized product was then oxidized with a stoichiometric amount of AgOTf in acetonitrile spiked with $H_2{}^{18}O$, followed by filtration and recrystallization from the acetonitrile solution by vapor diffusion of diethyl ether.

Synthesis of ^{18}O Isotopologue of 5. Complex **1** (40 mg, 0.04 mmol) was dissolved in 2 mL of acetonitrile spiked with $H_2{}^{18}O$ (~5 mg/mL) forming an orange solution. One drop of triethylamine (~10 mg, 0.1 mmol) was added to the solution turning it bright red immediately. The solution was left to stir for 1 h and then concentrated to ~1 mL volume, and the ^{18}O isotopologue of **2** was recrystallized from vapor diffusion of diethyl ether into acetonitrile. The recrystallized product was then reacted with 1,8-Diazabicyclo[5.4.0]undec-7-ene (DBU) to form the ^{18}O isotopologue of **3** as a precipitate from acetonitrile. Filtration of the suspension over diatomaceous earth and addition of a stoichiometric amount of AgOTf to the filter pad, followed by addition of 1 mL of acetonitrile spiked with $H_2{}^{18}O$ to the filter formed a solution of the ^{18}O isotopologue of **5** which was recrystallized from the acetonitrile solution by vapor diffusion of diethyl ether.

Rebound Hydroxylation using Gomberg's dimer and 4. To a 20 mL scintillation vial was added **4** (0.0202 g, 0.020 mmol), a stir bar, and 2 mL of acetonitrile. In a separate vial Gomberg's dimer (0.0057 g, 0.010 mmol, 0.5 equiv) was dissolved in 2 mL of tetrahydrofuran and added to the vial containing **4**. The reaction quickly turned from a dark red-brown solution to a bright yellow solution. After 0.5 h of stirring, volatiles were removed under reduced pressure and a yellow powder was triturated with diethyl ether. The ether-soluble products were separated and dried. The resulting white powder was dissolved in 2 mL of tetrahydrofuran containing a known amount of mesitylene as an internal standard. The formation of triphenylmethanol was observed by GC−MS and ^{1}H NMR analyses (Yield: 0.0052 g, 0.020 mmol, 99%). Quantification of triphenylmethanol by GC−MS was achieved through the use of a standard curve containing mesitylene as a standard.

■ ASSOCIATED CONTENT

Supporting Information

The Supporting Information is available free of charge on the ACS Publications website at DOI: 10.1021/jacs.9b01516.

Experimental spectra and crystallographic information (CIF)

Experimental spectra and crystallographic information (CIF)

Experimental spectra and crystallographic information (CIF)

Experimental spectra and crystallographic information (CIF)

Experimental spectra and crystallographic information (CIF)

Experimental data (PDF)

■ AUTHOR INFORMATION

Corresponding Author

*fout@illinois.edu.

ORCID

Michael J. Drummond: 0000-0002-1912-5116
Courtney L. Ford: 0000-0002-1509-4850
Danielle L. Gray: 0000-0003-0059-2096
Codrina V. Popescu: 0000-0003-2369-3383
Alison R. Fout: 0000-0002-4669-5835

Notes

The authors declare no competing financial interest.

DOI: 10.1021/jacs.9b01516
J. Am. Chem. Soc. XXXX, XXX, XXX−XXX

■ ACKNOWLEDGMENTS

This work was supported by the U.S. Department of Energy, Office of Science, Office of Basic Energy Sciences, Chemical Sciences, Geosciences and Biosciences Division under award DE-SC-0016026. The Mössbauer study is supported by start-up funds from The College of Arts and Sciences at The University of St. Thomas to CVP. The authors would like to thank M. J. Nilges for assistance with EPR spectroscopy and T. B. Rauchfuss for useful discussions and feedback. A.R.F. is a Sloan Research Fellow and a Camille Dreyfus Teacher-Scholar.

■ REFERENCES

(1) Rohde, J.-U.; In, J.-H.; Lim, M. H.; Brennessel, W. W.; Bukauski, M. R.; Stubna, A.; Münck, E.; Nam, W.; Que, L. Crystallographic and Spectroscopic Characterization of a Nonheme Fe(IV)═O Complex. *Science* **2003**, *299*, 1037−1039.
(2) Nam, W. Synthetic Mononuclear Nonheme Iron-Oxygen Intermediates. *Acc. Chem. Res.* **2015**, *48*, 2415−2423.
(3) Puri, M.; Que, L. Toward the Synthesis of More Reactive S = 2 Non-Heme Oxoiron(IV) Complexes. *Acc. Chem. Res.* **2015**, *48*, 2443−2452.
(4) Nam, W.; Lee, Y. M.; Fukuzumi, S. Tuning Reactivity and Mechanism in Oxidation Reactions by Mononuclear Nonheme Iron(IV)-Oxo Complexes. *Acc. Chem. Res.* **2014**, *47*, 1146−1154.
(5) Sahu, S.; Goldberg, D. P. Activation of Dioxygen by Iron and Manganese Complexes: A Heme and Nonheme Perspective. *J. Am. Chem. Soc.* **2016**, *138*, 11410−11428.
(6) Price, J. C.; Barr, E. W.; Tirupati, B.; Bollinger, J. M.; Krebs, C. The First Direct Characterization of a High-Valent Iron Intermediate in the Reaction of an α-Ketoglutarate-Dependent Dioxygenase: A High-Spin Fe(IV) Complex in Taurine/α-Ketoglutarate Dioxygenase (TauD) from Escherichia Coli. *Biochemistry* **2003**, *42*, 7497−7508.
(7) Krebs, C.; Fujimori, D. G.; Walsh, C. T.; Bollinger, J. M. Non-Heme Fe (IV)− Oxo Intermediates. *Acc. Chem. Res.* **2007**, *40*, 484−492.
(8) Meunier, B.; de Visser, S. P.; Shaik, S. Mechanism of Oxidation Reactions Catalyzed by Cytochrome P450 Enzymes. *Chem. Rev.* **2004**, *104*, 3947−3980.
(9) Bollinger, J. M.; Price, J. C.; Hoffart, L. M.; Barr, E. W.; Krebs, C. Mechanism of Taurine: α-Ketoglutarate Dioxygenase (TauD) from Escherichia Coli. *Eur. J. Inorg. Chem.* **2005**, *21*, 4245−4254.
(10) Martinez, S.; Hausinger, R. P. Catalytic Mechanisms of Fe (II) and 2-Oxoglutarate-Dependent Oxygenases. *J. Biol. Chem.***2015**, *290*, 20702−20711.
(11) Price, J. C.; Barr, E. W.; Glass, T. E.; Krebs, C.; Bollinger, J. M. Evidence for Hydrogen Abstraction from C1 of Taurine by the High-Spin Fe (IV) Intermediate Detected during Oxygen Activation by Taurine: α-Ketoglutarate Dioxygenase (TauD). *J. Am. Chem. Soc.* **2003**, *125*, 13008−13009.
(12) Proshlyakov, D. A.; Mccracken, J.; Hausinger, R. P. Spectroscopic Analyses of 2-oxoglutarate-Dependent Oxygenases: TauD as a Case Study. *J. Biol. Inorg. Chem.***2017**, *22*, 367−379.
(13) de Visser, S. P. Propene Activation by the Oxo-Iron Active Species of Taurine/α-Ketoglutarate Dioxygenase (TauD) Enzyme. How Does the Catalysis Compare to Heme-Enzymes? *J. Am. Chem. Soc.* **2006**, *128*, 9813−9824.
(14) de Visser, S. P. Differences in and Comparison of the Catalytic Properties of Heme and Non-Heme Enzymes with a Central Oxo−Iron Group. *Angew. Chem., Int. Ed.* **2006**, *45*, 1790−1793.
(15) Latifi, R.; Bagherzadeh, M.; de Visser, S. P. Origin of the Correlation of the Rate Constant of Substrate Hydroxylation by Nonheme Iron (IV)− Oxo Complexes with the Bond-Dissociation Energy of the C-H Bond of the Substrate. *Chem. - Eur. J.* **2009**, *15*, 6651−6662.
(16) Ye, S.; Neese, F. Nonheme Oxo-Iron (IV) Intermediates Form an Oxyl Radical upon Approaching the C−H Bond Activation Transition State. *Proc. Natl. Acad. Sci. U. S. A.***2011**, *108*, 1228−1233.
(17) Mai, B. K.; Kim, Y. Is It Fe (III)-Oxyl Radical That Abstracts Hydrogen in the C−H Activation of TauD? A Theoretical Study Based on the DFT Potential Energy Surfaces. *Inorg. Chem.* **2016**, *55*, 3844−3852.
(18) Mitchell, A. J.; Dunham, N. P.; Martinie, R. J.; Bergman, J. A.; Pollock, C. J.; Hu, K.; Allen, B. D.; Chang, W.; Silakov, A.; Bollinger, J. M.; Krebs, C.; Boal, A. K. Visualizing the Reaction Cycle in an Iron(II) and 2-(Oxo)-Glutarate- Dependent Hydroxylase. *J. Am. Chem. Soc.* **2017**, *139*, 13830−13836.
(19) Topf, M.; Sandala, G. M.; Smith, D. M.; Schofield, C. J.; Easton, C. J.; Radom, L. The Unusual Bifunctional Catalysis of Epimerization and Desaturation by Carbapenem Synthase. *J. Am. Chem. Soc.* **2004**, *126*, 9932−9933.
(20) Dunham, N. P.; Chang, W.; Mitchell, A. J.; Martinie, R. J.; Zhang, B.; Bergman, J. A.; Rajakovich, L. J.; Wang, B.; Silakov, A.; Krebs, C.; Boal, A. K.; Bollinger, M. J. Two Distinct Mechanisms for C−C Desaturation by Iron(II)- and 2-(Oxo)Glutarate-Dependent Oxygenases: Importance of α-Heteroatom Assistance. *J. Am. Chem. Soc.* **2018**, *140*, 7116−7126.
(21) Dunham, N. P.; Mitchell, A. J.; Del Río Pantoja, J. M.; Krebs, C.; Bollinger, M. J.; Boal, A. K. α-Amine Desaturation of D-Arginine by the Iron(II)- and 2-(Oxo)Gluterate-Dependent L-Arginine 3-Hydroxylase, VioC. *Biochemistry* **2018**, *57*, 6479−6488.
(22) Zhou, J.; Kelly, W. L.; Bachmann, B. O.; Gunsior, M.; Townsend, C. A.; Solomon, E. I. Spectroscopic Studies of Substrate Interactions with Clavaminate Synthase 2, a Multifunctional α-KG-Dependent Non-Heme Iron Enzyme: Correlation with Mechanisms and Reactivities. *J. Am. Chem. Soc.* **2001**, *123*, 7388−7398.
(23) Huang, J.; Tang, Y.; Yu, C.; Sanyal, D.; Jia, X.; Liu, X.; Guo, Y.; Chang, W. Mechanistic Investigation of Oxidative Decarboxylation Catalyzed by Two Iron(II)- and 2-Oxoglutarate-Dependent Enzymes. *Biochemistry* **2018**, *57*, 1838−1841.
(24) Blasiak, L. C.; Drennan, C. L. Structural Perspective on Enzymatic Halogenation. *Acc. Chem. Res.* **2009**, *42*, 147−155.
(25) Ogo, S.; Wada, S.; Watanabe, Y.; Iwase, M.; Wada, A.; Harata, M.; Jitsukawa, K.; Masuda, H.; Einaga, H. Synthesis, Structure, and Spectroscopic Properties of [Fe(III)(Tnpa)(OH)(PhCOO)ClO_4: A Model Complex for an Active Form of Soybean Lipoxygenase-1. *Angew. Chem., Int. Ed.* **1998**, *37*, 2102−2104.
(26) MacBeth, C. E.; Golombek, A. P.; Young, V. G.; Yang, C.; Kuczera, K.; Hendrich, M. P.; Borovik, A. S. O_2 Activation by Nonheme Iron Complexes: A Monomeric Fe(III)- Oxo Complex Derived from O_2. *Science* **2000**, *289*, 938−941.
(27) Soo, H. S.; Komor, A. C.; Iavarone, A. T.; Chang, C. J. A Hydrogen-Bond Facilitated Cycle for Oxygen Reduction by an Acid- and Base-Compatible Iron Platform. *Inorg. Chem.* **2009**, *48*, 10024−10035.
(28) Cook, S. A.; Ziller, J. W.; Borovik, A. S. Iron(II) Complexes Supported by Sulfonamido Tripodal Ligands: Endogenous versus Exogenous Substrate Oxidation. *Inorg. Chem.* **2014**, *53*, 11029−11035.
(29) Yeh, C. Y.; Chang, C. J.; Nocera, D. G. Hangman" Porphyrins for the Assembly of a Model Heme Water Channel. *J. Am. Chem. Soc.* **2001**, *123*, 1513−1514.
(30) MacBeth, C. E.; Hammes, B. S.; Young, V. G.; Borovik, A. S. Hydrogen-Bonding Cavities about Metal Ions: Synthesis, Structure, and Physical Properties for a Series of Monomeric M-OH Complexes Derived from Water. *Inorg. Chem.* **2001**, *40*, 4733−4741.
(31) Ogo, S.; Yamahara, R.; Roach, M.; Suenobu, T.; Aki, M.; Ogura, T.; Kitagawa, T.; Masuda, H.; Fukuzumi, S.; Watanabe, Y. Structural and Spectroscopic Features of a Cis (Hydroxo)-FeIII-(Carboxylato) Configuration as an Active Site Model for Lipoxygenases. *Inorg. Chem.* **2002**, *41*, 5513−5520.
(32) MacBeth, C. E.; Gupta, R.; Mitchell-Koch, K. R.; Young, V. G.; Lushington, G. H.; Thompson, W. H.; Hendrich, M. P.; Borovik, A. S. Utilization of Hydrogen Bonds to Stabilize M-O(H) Units: Synthesis and Properties of Monomeric Iron and Manganese Complexes with Terminal Oxo and Hydroxo Ligands. *J. Am. Chem. Soc.* **2004**, *126*, 2556−2567.

DOI: 10.1021/jacs.9b01516
J. Am. Chem. Soc. XXXX, XXX, XXX−XXX

(33) Harman, W. H.; Chang, C. J. N_2O Activation and Oxidation Reactivity from a Non-Heme Iron Pyrrole Platform. *J. Am. Chem. Soc.* **2007**, *129*, 15128−15129.
(34) Çelenligil-Çetin, R.; Paraskevopoulou, P.; Dinda, R.; Staples, R. J.; Sinn, E.; Rath, N. P.; Stavropoulos, P. Synthesis, Characterization, and Reactivity of Iron Trisamidoamine Complexes That Undergo Both Metal- and Ligand-Centered Oxidative Transformations. *Inorg. Chem.* **2008**, *47*, 1165−1172.
(35) Mukherjee, J.; Lucas, R. L.; Zart, M. K.; Powell, D. R.; Day, V. W.; Borovik, A. S. Synthesis, Structure, and Physical Properties for a Series of Monomeric Iron(III) Hydroxo Complexes with Varying Hydrogen-Bond Networks. *Inorg. Chem.* **2008**, *47*, 5780−5786.
(36) Zaragoza, J. P. T.; Yosca, T. H.; Siegler, M. A.; Moenne-Loccoz, P.; Green, M. T.; Goldberg, D. P. Direct Observation of Oxygen Rebound with an Iron-Hydroxide Complex. *J. Am. Chem. Soc.* **2017**, *139*, 13640−13643.
(37) Pangia, T. M.; Davies, C. G.; Prendergast, J. R.; Gordon, J. B.; Siegler, M. A.; Jameson, G. N. L.; Goldberg, D. P. Observation of Radical Rebound in a Mononuclear Nonheme Iron Model Complex. *J. Am. Chem. Soc.* **2018**, *140*, 4191−4194.
(38) Matson, E. M.; Bertke, J. A.; Fout, A. R. Isolation of Iron(II) Aqua and Hydroxyl Complexes Featuring a Tripodal H-Bond Donor and Acceptor Ligand. *Inorg. Chem.* **2014**, *53*, 4450−4458.
(39) Matson, E. M.; Park, Y. J.; Bertke, J. A.; Fout, A. R. Synthesis and Characterization of M(II) (M = Mn, Fe and Co) Azafulvene Complexes and Their X_3^- Derivatives. *Dalt. Trans.* **2015**, *44*, 10377−10384.
(40) Park, Y. J.; Matson, E. M.; Nilges, M. J.; Fout, A. R. Exploring Mn−O Bonding in the Context of an Electronically Flexible Secondary Coordination Sphere: Synthesis of a Mn(III)−Oxo. *Chem. Commun.* **2015**, *51*, 5310−5313.
(41) Sahu, S.; Widger, L. R.; Quesne, M. G.; De Visser, S. P.; Matsumura, H.; Moënne-Loccoz, P.; Siegler, M. A.; Goldberg, D. P. Secondary Coordination Sphere Influence on the Reactivity of Nonheme Iron(II) Complexes: An Experimental and DFT Approach. *J. Am. Chem. Soc.* **2013**, *135*, 10590−10593.
(42) Widger, L. R.; Davies, C. G.; Yang, T.; Siegler, M. A.; Troeppner, O.; Jameson, G. N. L.; Ivanović-Burmazović, I.; Goldberg, D. P. Dramatically Accelerated Selective Oxygen-Atom Transfer by a Nonheme Iron(IV)-Oxo Complex: Tuning of the First and Second Coordination Spheres. *J. Am. Chem. Soc.* **2014**, *136*, 2699−2702.
(43) Widger, L. R.; Jiang, Y.; McQuilken, A. C.; Yang, T.; Siegler, M. A.; Matsumura, H.; Moënne-Loccoz, P.; Kumar, D.; de Visser, S. P.; Goldberg, D. P. Thioether-Ligated Iron(II) and Iron(III)-Hydroperoxo/Alkylperoxo Complexes with an H-Bond Donor in the Second Coordination Sphere. *Dalt. Trans.* **2014**, *43*, 7522.
(44) Hart, J. S.; Nichol, G. S.; Love, J. B. Directed Secondary Interactions in Transition Metal Complexes of Tripodal Pyrrole Imine and Amide Ligands. *Dalt. Trans.* **2012**, *41*, 5785−5788.
(45) Peters, G. M.; Winegrad, J. B.; Gau, M. R.; Imler, G. H.; Xu, B.; Ren, S.; Wayland, B. B.; Zdilla, M. J. Synthesis and Structure of 2,5-Bis[N-(2,6-Mesityl)Iminomethyl]Pyrrolylcobalt(II): Evidence for One-Electron- Oxidized, Redox Noninnocent Ligand Behavior. *Inorg. Chem.* **2017**, *56*, 3377−3385.
(46) Hikichi, S.; Ogihara, T.; Fujisawa, K.; Kitajima, N.; Akita, M.; Moro-oka, Y. Synthesis and Characterization of the Benzoylformato Ferrous Complexes with the Hindered Tris(Pyrazolyl)Borate Ligand as a Structural Model for Mononuclear Non-Heme Iron Enzymes. *Inorg. Chem.* **1997**, *36*, 4539−4547.
(47) Bénisvy, L.; Halut, S.; Donnadieu, B.; Tuchagues, J. P.; Chottard, J. C.; Li, Y. Monomeric Iron(II) Hydroxo and Iron(III) Dihydroxo Complexes Stabilized by Intermolecular Hydrogen Bonding. *Inorg. Chem.* **2006**, *45*, 2403−2405.
(48) Kendall, A. J.; Zakharov, L. N.; Gilbertson, J. D. Synthesis and Stabilization of a Monomeric Iron(II) Hydroxo Complex via Intra Molecular Hydrogen Bonding in the Secondary Coordination Sphere. *Inorg. Chem.* **2010**, *49*, 8656−8658.
(49) Gordon, Z.; Drummond, M. J.; Matson, E. M.; Bogart, J. A.; Schelter, E. J.; Lord, R. L.; Fout, A. R. Tuning the Fe(II/III) Redox Potential in Nonheme Fe(II)-Hydroxo Complexes through Primary and Secondary Coordination Sphere Modifications. *Inorg. Chem.* **2017**, *56*, 4852−4863.
(50) Kaljurand, I.; Kutt, A.; Soovali, L.; Rodima, T; Maemets, V.; Leito, I.; Koppel, I. A. Extension of the Self-Consistent Spectrophotometric Basicity Scale in Acetonitrile to a Full Span of 28 p K a Units: Unification of Different Basicity Scales. *J. Org. Chem.* **2005**, *70*, 1019−1028.
(51) Gupta, R.; Borovik, A. S. Monomeric MnIII/II and FeIII/II Complexes with Terminal Hydroxo and Oxo Ligands: Probing Reactivity via O-H Bond Dissociation Energies. *J. Am. Chem. Soc.* **2003**, *125*, 13234−13242.
(52) Matson, E. M.; Park, Y. J.; Fout, A. R. Facile Nitrite Reduction in a Non-Heme Iron System: Formation of an Iron(III)-Oxo. *J. Am. Chem. Soc.* **2014**, *136*, 17398−17401.
(53) Gütlich, P.; Bill, E.; Trautwein, A. X. *Mössbauer Spectroscopy and Transition Metal Chemistry Fundamentals and Application*; Springer-Verlag: Berlin/Heidelberg, 2011.
(54) Ching, W.; Zhou, A.; Klein, J. E. M. N.; Fan, R.; Knizia, G.; Cramer, C. J.; Guo, Y.; Que, L. Characterization of the Fleeting Hydroxoiron (III) Complex of the Pentadentate TMC-Py Ligand. *Inorg. Chem.* **2017**, *56*, 11129−11140.
(55) Warren, J. J.; Tronic, T. A.; Mayer, J. M. Thermochemistry of Proton-Coupled Electron Transfer Reagents and Its Implications. *Chem. Rev.* **2010**, *110*, 6961−7001.
(56) Usharani, D.; Lacy, D. C.; Borovik, A. S.; Shaik, S. Dichotomous Hydrogen Atom Transfer vs Proton-Coupled Electron Transfer During Activation of X−H Bonds (X = C, N, O) by Nonheme Iron−Oxo Complexes of Variable Basicity. *J. Am. Chem. Soc.* **2013**, *135*, 17090−17104.
(57) Guengerich, F. P. Mechanisms of Cytochrome P450-Catalyzed Oxidations. *ACS Catal.* **2018**, *8*, 10964−10976.
(58) Ishikawa, N.; Tanaka, H.; Koyama, F.; Noguchi, H.; Wang, C. C. C.; Hotta, K.; Watanabe, K. Non-Heme Dioxygenase Catalyzes Atypical Oxidations of 6,7-Bicyclic Systems To Form the 6, 6-Quinolone Core of Viridicatin-Type Fungal Alkaloids. *Angew. Chem., Int. Ed.* **2014**, *53*, 12880−12884.
(59) Bräuer, A.; Beck, P.; Hintermann, L.; Groll, M. Structure of the Dioxygenase AsqJ: Mechanistic Insights into a One- Pot Multistep Quinolone Antibiotic Biosynthesis. *Angew. Chem., Int. Ed.* **2016**, *55*, 422−426.
(60) Nakashima, Y.; Mori, T.; Nakamura, H.; Awakawa, T.; Hoshino, S.; Senda, M.; Senda, T.; Abe, I. Structure Function and Engineering of Multifunctional Non-Heme Iron Dependent Oxygenases Oxygenases in Fungal Meroterpenoid Biosynthesis. *Nat. Commun.* **2018**, *9*, 1−10.
(61) Meng, S.; Han, W.; Zhao, J.; Jian, X.; Pan, H.; Tang, G. A Six-Oxidase Cascade for Tandem C-H Bond Activation Revealed by Reconstitution of Bicyclomycin Biosynthesis Communications Angewandte. *Angew. Chem., Int. Ed.* **2018**, *57*, 719−723.
(62) Hagadorn, J. R.; Que, L.; Tolman, W. B. N-Donor Effects on Carboxylate Binding in Mononuclear Iron (II) Complexes of a Sterically Hindered Benzoate Ligand. *Inorg. Chem.* **2000**, *39*, 6086−6090.
(63) Curley, J. J.; Bergman, G.; Tilley, T. D. Preparation and Physical Properties of Early-Late Heterobimetallic Compounds. *Dalt. Trans.* **2012**, *41*, 192−200.
(64) Zong, R.; Wang, D.; Hammitt, R.; Thummel, R. P. Synthetic Approaches to Polypyridyl Bridging Ligands with Proximal Multidentate Binding Sites. *J. Org. Chem.* **2006**, *71*, 167−175.
(65) Ünal, E. A.; Wiedemann, D.; Seiffert, J.; Boyd, J. P.; Grohmann, A. Efficient Synthesis of Pentakis- and Tris(Pyridine) Ligands. *Tetrahedron Lett.* **2012**, *53*, 54−55.

DOI: 10.1021/jacs.9b01516
J. Am. Chem. Soc. XXXX, XXX, XXX−XXX